Numerical Study of Interrupted Impinging Jets for Cooling of Electronics

Ramesh Chandra Behera, Pradip Dutta, and K. Srinivasan

***Abstract*—The objective of this paper is to present the results of a numerical investigation of the effect of flow pulsations on local, time-averaged Nusselt number of an impinging air jet. The problem was considered to provide inputs to augmenting heat transfer from electronic components. The solution is sought through the FLUENT (Version 6.0) platform. The standard k-ϵ model for turbulence equations and two-layer zonal model in wall function are used in the problem. Pressure-velocity coupling is handled using the SIMPLEC algorithm. The model is first validated against some experimental results available in the literature. A parametric study is carried out to quantify the effect of the pulsating jets. The parameters considered are 1) average jet Reynolds number ($5130 < Re < 8560$), 2) sine and square wave pulsations, 3) frequencies of pulsations ($25 < f < 400$ Hz), and 4) height of impingement to jet diameter ratios ($5 < H/d < 9$). In the case of sine wave pulsations, the ratio of root mean square value of the amplitude to the average value (A_N) was varied from 18% to 53%. The studies are restricted to a constant wall heat flux condition. Parametric conditions for which enhancement in the time-averaged heat transfer from the surface can be expected are identified.**

***Index Terms*—Heat flux condition, impinging air jet, pulsating jet.**

NOMENCLATURE

$A_N(\%)$	Pulse amplitude ($= (u_{\rm rms}/u_{\rm avg}) \times 100$).
c_p	Fluid specific heat (J kg^{-1}K^{-1}).
d	Diameter of circular nozzle (m).
f	Frequency of the pulsating jet (Hz).
G_k	Production of turbulent kinetic energy (m^{2}s^{-3}).
h	Convective heat transfer coefficient (W m^{-2}K^{-1}).
H	Height of nozzle-to-wall spacing (m).
k	Turbulent kinetic energy (m^{2}s^{-2}).
K	Fluid thermal conductivity (W m^{-1}K^{-1}).
L	Length of the wall (m).
Nu	Nusselt number based on nozzle diameter $[= (hd/K) = (q/(T_w - T_\infty))(d/K)]$.
p	Pressure (N m^{-2}).
Pr	Fluid prandtl number.
Pr_t	Turbulent prandtl number ($= 0.85$).
q	Wall heat flux (W m^{-2}).
Re	Reynolds number based on nozzle diameter $(= (\rho u_{\rm avg} d/\mu))$.
t	Time (s).
T	Time period (s).
T	Temperature (K).
u, ν	Velocities in x, and r directions (m s^{-1}).
$u_{\rm avg}$	Time-averaged velocity component of a pulsating jet (m s^{-1}).
$u_{\rm amp}$	Periodic velocity component of a sine wave jet (m s^{-1}).
$u_{\rm jet}$	Jet velocity (m s^{-1}).
$u_{\rm peak}$	Maximum velocity component of a square wave jet (m s^{-1}).
$u_{\rm rms}$	Root mean square value of the $u_{\rm amp}$ (m s^{-1}).
u'	Turbulent velocity component (m s^{-1}).
r, x	Coordinate axes.

Greek Symbols

ε	Dissipation rate of kinetic energy (m^{2}s^{-3}).
κ	Von Karman's constant ($= 0.42$).
μ	Fluid dynamic viscosity (kg m^{-1}s^{-1}).
μ_t	Turbulent viscosity (kg m^{-1}s^{-1}).
ρ	Fluid density (kg m^{-3}).
τ	Shear stress (N m^{-2}).
Δ	Hydrodynamic boundary layer thickness (m).

Subscripts

avg	Time-averaged value.
amp	Periodic value.
peak	Maximum value.
rms	Root mean square value.
s	Stagnation point.
r	Radial.
x	Axial.
w	Wall value.

Superscripts

$'$	Turbulent value.

Manuscript received May 20, 2004; revised March 21, 2005. This work was supported by a Defence Research and Development Organization, Government of India Grant-in-Aid. This work was recommended for publication by Associate Editor P. Sathyamurthy upon evaluation of the reviewers comments.

The authors are with the Department of Mechanical Engineering, Indian Institute of Science, Bangalore 560012, India (e-mail: mecks@mecheng.iisc.ernet.in; mecks@hotmail.com).

Digital Object Identifier 10.1109/TCAPT.2007.898353

I. Introduction

IMPINGING jets have been used extensively in thermal systems such as drying, manufacture of steel, turbine-blades, etc for enhancement of heat transfer. More specifically, in the thermal management of electronic components, increased power dissipation in chips with ever higher component-densities has propelled the use of impinging jets to augment cooling. If the performance of impinging jets can be further enhanced, there will be a potential for an increase in the electronic component's life span.

There is an excellent compilation of literature on enhancing the convective heat transfer coefficient with steady impinging jets [1], [2]. Parameters that influence the magnitude of enhancement are the height and angle of impingement and turbulence intensity. A steady impinging jet stabilizes the boundary layer on the surface to be cooled. A further enhancement in the convective heat transfer coefficient is possible if the boundary layer can be disrupted. One method of achieving this is by pulsating the jet, i.e., making it unsteady. The speed of pulsation should be such that the boundary layer can be disturbed and yet adequate coolant is made available.

Some of the possible features that could cause the enhancement due to pulsed jets are: a) higher turbulence promoted by flow instabilities at the free surface, b) chaotic mixing which promotes entrainment, and c) reduced resistance of the boundary layer growth on the impingement surface. The nonlinear dynamic response of the hydrodynamic and thermal boundary layers to flow pulsations has been investigated recently [3].

Zumbrunnen and Aziz [4] were, perhaps, the first to study the importance of pulsation frequency and amplitude. They investigated convective heat transfer with a planar impinging water jet (50.8 $\times$ 5.08 mm) on a surface subjected to a constant heat flux. Their experiments covered Reynolds numbers ranging from 3300 to 19600 and frequencies up to 142 Hz. A two fold enhancement of heat transfer was reported. They observed that, to be effective, the pulsation frequency must be of the order of 100's of Hz. Experimental investigations were reported also by Mladin and Zumbrunnen [5] who studied the effect of flow pulsations on the local heat transfer coefficient of a planar jet at Reynolds numbers of 1000, 5500, and 11000, frequencies up to 82 Hz and with a nozzle outlet size of 50 $\times$ 5 mm. It was observed that Nusselt number enhancement depends on pulse frequency and amplitude in addition to Reynolds number and the impingement height. The largest Nusselt was observed at a H/w ratio between 7 and 8. Another investigation by them [6] brings out that the forcing Strouhal number is an influential parameter that controlled the large-scale structure formation and interaction, as well as downstream penetration distance, and a high value of Strouhal number may enhance cooling of electronic packages by surface renewal effects from large incident flow structures.

Further contributions in the area of multiple jets came from Sheriff and Zumbrunnen [7] by way of multiple orifices and convergent nozzle jets. They observed a greater heat transfer rate and a better heat transfer distribution in the latter case. The difference was 34%–38%. It was also brought out that the best results were obtained for a jet height to diameter ratio of 2. Flow pulsations appear to increase the time averaged boundary layer thickness and lead to reduction in heat transfer for pulsations in the region of 10–65 Hz frequency. They further concluded that at high pulsation frequencies, a more abundant succession of incident vortices was produced in the jet so that non-linear dynamical boundary layer effects became secondary to improved mixing.

Sheriff and Zumbrunnen [8] expanded the study to pulsating array of jets. An array of nine convergent jets in a square matrix was used to cover a Reynolds number range of 2 500–10 000, a jet height to diameter ratio of 2–6, pulse frequency up to 65 Hz, a Strouhal number of 0.028 and a flow pulsation magnitude up to 60%. Their conclusions were: 1) increased jet interactions at large magnitude of flow pulsations was found to reduce the jet potential core length by up to 20%, 2) turbulence intensities were higher by 7–15% than in steady jets, and 3) despite evidence of coherent flow structures and increased turbulence, stagnation Nusselt numbers were lower by 18% for a 60% pulse magnitude. The heat transfer rate was unchanged in the region away from the stagnation point.

Studies on the waveform of pulsations by Sheriff and Zumbrunnen [9] indicate that the time averaged stagnation Nusselt numbers reduced by 17% for sinusoidal pulsations for large pulse magnitudes and increased by 33% for square wave pulses. The experiments were conducted with water as the cooling medium. The frequency range covered was up to 280 Hz. The range of Reynolds numbers covered was 3150–15800.

The importance of duty cycle (i.e., the ratio of pulse cycle on-time to total cycle time) for a pulsated impinging jet was investigated by Sailor *et al.* [10]. They show that a duty cycle of 0.25 produces a better effect than at 0.33 or 0.50 for frequencies up to 60 Hz in the Reynolds number range of 21000–31000 and jet-to wall spacing ratios of 4–8.

Mladin and Zumbrunnen [3], [11] developed a mathematical model to study the nonlinear dynamics of the hydrodynamic and thermal boundary layers within a planar stagnation region. They conclude that high frequency, low amplitude fluctuations are better than low frequency, high amplitude fluctuations.

The present study is complementary to the above efforts on using pulsated jets in applications involving cooling of electronic systems. This paper focuses on axi-symmetric submerged air jet. The physical model of an impinging jet is shown in Fig. 1. Some lacuna of numerical investigations of the pulsated impinging jets sets the agenda for the present work. A systematic analysis of the influence of waveform, frequency of pulsating, height of impingement and Reynolds number is represented. The solution is obtained through the use of FLUENT 6.0 [12] as a solver for thermal and flow fields using the standard $k-\varepsilon$ turbulence model. The range covered is jet Reynolds number, 5130–8560, frequencies of interruptions from 0–400 Hz, and height to jet diameter ratios from 5 to 9. The studies are restricted to constant wall heat flux condition as this is the most common feature of cooling of electronic components.

II. Mathematical Formulation

The pulsated impinging jet heat transfer problem is numerically computed with the commercial finite-volume code

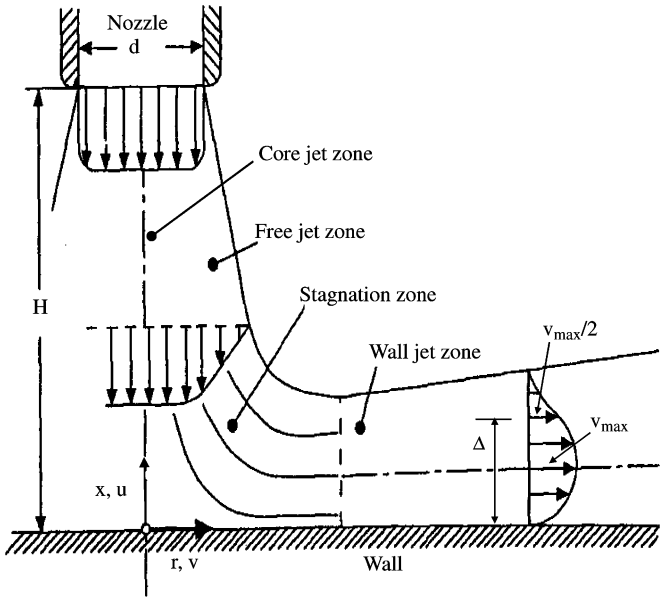

Fig. 1. Schematic diagram of an impingement jet flow field.

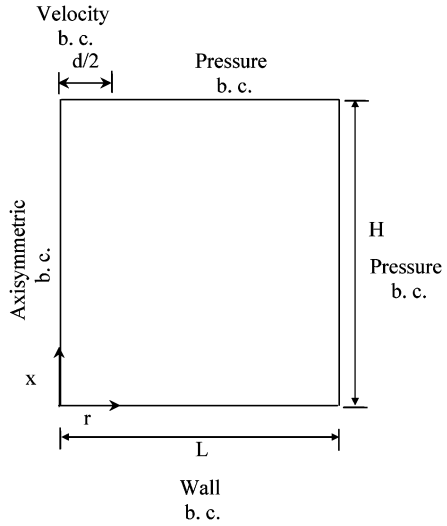

Fig. 2. Schematic illustration of the computational domain.

FLUENT 6.0 using the time-averaged Navier-Stokes and energy equations with the standard $k-\varepsilon$ turbulent model. The $k-\varepsilon$ model is chosen due to its simplicity, computational economy and wide acceptability.

The circular air jet is assumed to have constant thermophysical physical properties such as density, specific heat and thermal conductivity. Hence, the geometric boundaries and physical conditions are symmetric about the axis of the jet; a 2-D axi-symmetric model is constructed. It neglects gravitational effect during the impinging jet. The axi-symmetric domain is shown in Fig. 2. The equations for 2-D incompressible flow can be written as follows.

- Conservation of mass

$$\frac{\partial}{\partial x}(\rho u)+\frac{1}{r}\frac{\partial}{\partial r}(\rho r v)=0. \tag{1}$$

- Conservation of linear momentum
  For x-momentum

$$\begin{aligned}\frac{\partial}{\partial t}(\rho u)+\frac{1}{r}\frac{\partial}{\partial x}(\rho u r u)+\frac{1}{r}\frac{\partial}{\partial r}(\rho v r u)&=-\frac{\partial p}{\partial x}+\frac{1}{r}\frac{\partial}{\partial x}\left(r(\mu+\mu_t)\frac{\partial u}{\partial x}\right)+\frac{1}{r}\frac{\partial}{\partial r}\left(r(\mu+\mu_t)\frac{\partial u}{\partial r}\right)\\&\quad+\frac{\partial}{\partial x}\left(\mu_t\frac{\partial u}{\partial x}\right)+\frac{1}{r}\frac{\partial}{\partial r}\left(r\mu_t\frac{\partial v}{\partial x}\right)\end{aligned} \tag{2}$$

  and for r-momentum

$$\begin{aligned}\frac{\partial}{\partial t}(\rho v)+\frac{1}{r}\frac{\partial}{\partial x}(\rho u r v)+\frac{1}{r}\frac{\partial}{\partial r}(\rho v r v)&=-\frac{\partial p}{\partial r}-\frac{\mu v}{r^2}+\frac{1}{r}\frac{\partial}{\partial x}\left(r(\mu+\mu_t)\frac{\partial v}{\partial x}\right)\\&\quad+\frac{1}{r}\frac{\partial}{\partial r}\left(r(\mu+\mu_t)\frac{\partial v}{\partial r}\right)+\frac{\partial}{\partial x}\left(\mu_t\frac{\partial u}{\partial r}\right)\\&\quad+\frac{1}{r}\frac{\partial}{\partial r}\left(r\mu_t\frac{\partial v}{\partial r}\right).\end{aligned} \tag{3}$$

- Energy conservation

$$\begin{aligned}\frac{\partial}{\partial t}(\rho c_p T)+\frac{1}{r}\frac{\partial}{\partial x}\left[ur(\rho c_p T+p)\right]+\frac{1}{r}\frac{\partial}{\partial r}\left[vr(\rho c_p T+p)\right]&=\frac{1}{r}\frac{\partial}{\partial x}\left(r\left(K+\frac{c_p\mu_t}{\mathrm{Pr}_t}\right)\frac{\partial T}{\partial x}\right)\\&\quad+\frac{1}{r}\frac{\partial}{\partial r}\left(r\left(K+\frac{c_p\mu_t}{\mathrm{Pr}_t}\right)\frac{\partial T}{\partial r}\right).\end{aligned} \tag{4}$$

- The Standard $k-\varepsilon$ Turbulent Model

$$\begin{aligned}\frac{\partial}{\partial t}(\rho k)+\frac{1}{r}\frac{\partial}{\partial x}(\rho u r k)+\frac{1}{r}\frac{\partial}{\partial r}(\rho v r k)&=\frac{1}{r}\frac{\partial}{\partial x}\left[r\left(\mu+\frac{\mu_t}{\sigma_k}\right)\frac{\partial k}{\partial x}\right]\\&\quad+\frac{1}{r}\frac{\partial}{\partial r}\left[r\left(\mu+\frac{\mu_t}{\sigma_k}\right)\frac{\partial k}{\partial r}\right]+G_k-\rho\varepsilon\end{aligned} \tag{5}$$

  and

$$\begin{aligned}\frac{\partial}{\partial t}(\rho\varepsilon)+\frac{1}{r}\frac{\partial}{\partial x}(\rho u r\varepsilon)+\frac{1}{r}\frac{\partial}{\partial r}(\rho v r\varepsilon)&=\frac{1}{r}\frac{\partial}{\partial x}\left[r\left(\mu+\frac{\mu_t}{\sigma_\varepsilon}\right)\frac{\partial \varepsilon}{\partial x}\right]\\&\quad+\frac{1}{r}\frac{\partial}{\partial r}\left[r\left(\mu+\frac{\mu_t}{\sigma_\varepsilon}\right)\frac{\partial \varepsilon}{\partial r}\right]+C_{1\varepsilon}G_k\frac{\varepsilon}{k}-C_{2\varepsilon}\rho\frac{\varepsilon^2}{k}\end{aligned} \tag{6}$$

  where the values for the empirical constants are $C_{1\varepsilon}=1.44$, $C_{2\varepsilon}=1.92$, $\sigma_k=1.0$ and $\sigma_e=1.3$.

The term G_k is the volumetric rate of generation of turbulent kinetic energy and is defined as

$$G_k=\mu\left[2\left\{\left(\frac{\partial u}{\partial x}\right)^2+\left(\frac{\partial v}{\partial r}\right)^2+\left(\frac{v}{r}\right)^2\right\}+\left(\frac{\partial u}{\partial r}+\frac{\partial v}{\partial x}\right)^2\right]. \tag{7}$$

The turbulent viscosity (μ_t) term is defined as

$$\mu_t=\rho C_\mu\frac{k^2}{\varepsilon} \tag{8}$$

where the value of empirical constant, C_μ is 0.09.

Initial and Boundary Conditions: The boundary conditions adopted for solution of the governing equations are:

a) Velocity boundary condition at the inlet of the domain:

The jet velocity is assumed to be steady or pulsated with respect to time. The type of the pulsation waveform of the jet velocity is shown in Fig. 3 and is discussed subsequently.

A steady jet is defined as

$$u_{\text{jet}} = u_{\text{avg}}. \tag{9}$$

A jet with sinusoidal waveform can be described as

$$u_{\text{jet}} = u_{\text{avg}} + u_{\text{amp}} \sin(2\pi \text{ft}) \tag{10}$$

where $u_{\text{avg}} > u_{\text{amp}}$.

A jet with a square waveform can be described as

$$u_{\text{jet}} = \begin{cases} u_{\text{peak}} & \text{for} \quad t = (2n+1)\frac{T}{2} \\ 0 & \text{for} \quad t = 2n\frac{T}{2} \end{cases} \tag{11}$$

where $u_{\text{avg}} = (u_{\text{peak}}/2)$ and $n = 0,1,2,3,4,5, \ldots\ldots$.

The turbulent kinetic energy, k is calculated as

$$k = \frac{3}{2}(u_{\text{jet}} I)^2 \tag{12}$$

where the turbulent intensity (I) is defined as

$$I = \frac{u'_{\text{rms}}}{u_{\text{avg}}} = 0.16\text{Re}^{\frac{-1}{8}} \tag{13}$$

where u'_{rms} and u_{avg} are the root-mean-square (rms) of the velocity fluctuations (u') and time-average of the velocity component (u) respectively.

The dissipation rate, ε, is calculated as

$$\varepsilon = C_{\mu}^{\frac{3}{4}} \frac{k^{\frac{3}{2}}}{l} \tag{14}$$

where l is the turbulence length scale which is a physical quantity related to the size of the large eddies that contain the energy in turbulent flows. An approximate relationship between l and the physical size of the nozzle is defined as

$$l = 0.07 d_h \tag{15}$$

where d_h is the relevant dimension and it is equal to hydraulic diameter of the nozzle

The jet inlet temperature is constant and is same as atmospheric temperature (i.e., $T = T_{\infty}$).

b) Pressure boundary condition:
The boundary condition is imposed with constant atmospheric pressure and temperature:

$$p = p_{\infty}, \quad T = T_{\infty}, \quad \text{k} = \varepsilon = 0. \tag{16}$$

c) Wall boundary condition:
No-slip condition with constant heat flux is imposed at the wall boundaries.

d) Initial condition:
The initial conditions appropriate to the physical situations are as follows:

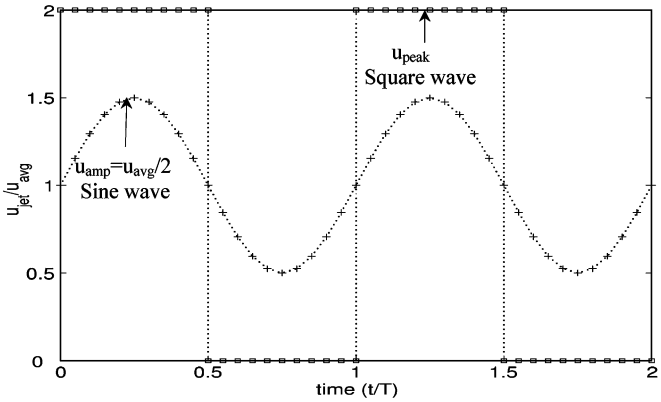

Fig. 3. Different waveforms of the impinging jet velocity.

$$\text{at} \quad t = 0, \qquad u = v = 0,\ p = p_{\infty},\ T = T_{\infty},\ k = \varepsilon = 0. \tag{17}$$

Treatment near wall: The two-layer zonal model is used in the wall function for numerical computations [13]. In two-layer zonal model, the whole domain is subdivided into a viscosity affected region and a fully turbulent region. The demarcation of the two regions is determined by a wall-distance based, turbulent Reynolds number (Re_x), is defined as

$$Re_x = \frac{\rho\sqrt{k}}{\mu} x \tag{18}$$

where x is the normal distance from the wall at the cell centers.

In the fully turbulent region (where Re_x >200), both k and ε equations are employed. In the viscosity-affected near-wall region (where Re_x <200), the k (5) is only employed. And instead of using (6), the ε is algebraically calculated as

$$\varepsilon = \frac{k^{\frac{3}{2}}}{\ell_{\varepsilon}}. \tag{19}$$

And instead of using (8), the turbulent viscosity (μ_t) is computed from

$$\mu_t = \rho C_{\mu} \sqrt{k} \ell_{\mu}. \tag{20}$$

The length scales (l_{ε} and l_{μ}) that appear in (19) and (20) are defined as [14]

$$\ell_{\varepsilon} = c_{\ell} x \left[1 - exp\left(-\frac{Re_x}{A_{\varepsilon}}\right)\right] \tag{21}$$

and

$$\ell_{\mu} = c_{\ell} x \left[1 - exp\left(-\frac{Re_x}{A_{\mu}}\right)\right] \tag{22}$$

The constants (c_l, A_{μ} and A_{ε}) are given by

$$c_{\ell} = \kappa C_{\mu}^{\frac{-3}{4}}, \quad A_{\mu} = 70, \quad A_{\varepsilon} = 2c_{\ell}. \tag{23}$$

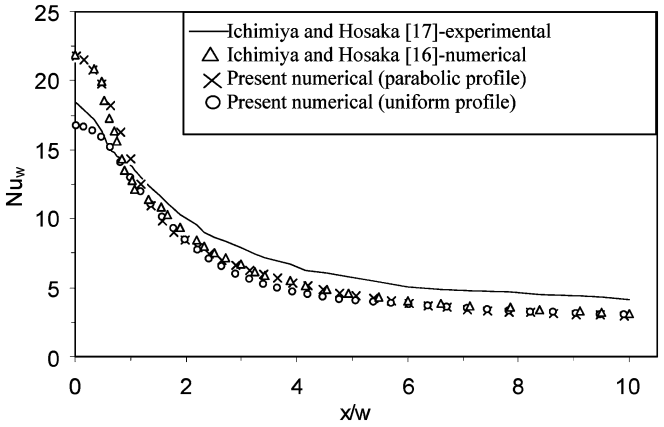

Fig. 4. Comparison of steady Nusselt number with numerical and experimental results [16], [17] for $Re_w = 500$, $H/w = 1$ and $q = 500$ wm^{-2}.

III. Numerical Procedure

The finite-volume code FLUENT 6.0 is used to solve the thermal and flow fields using the standard $k - \varepsilon$ turbulence model. Diffusion terms of all the governing equations are discretized using the central difference scheme. Convective terms of the momentum and energy equations are discretized using the third order QUICK interpolation scheme and convective terms of the turbulent kinetic energy and turbulent dissipation rate equations are discretized using a second-order upwind differencing scheme. Pressure-velocity coupling is handled using the SIMPLEC algorithm [15].

Near-wall meshing: Successful computation of the turbulent model requires some consideration during the mesh generation. Since turbulence plays a dominant role in the solving of transport equations, it must be ensured that turbulence quantities are properly resolved. It is therefore proposed to use sufficiently fine meshes to resolve the near-wall region sufficiently. Hence, the following meshing requirements are adopted.

a) A two-layer zonal model is employed for resolving the laminar sublayer, x^+ value should be within 4 to 5 at the cell adjacent to the wall. x^+ is defined as:

$$x^+ = \frac{\rho v_\tau x}{\mu} \tag{24}$$

where ν_τ is the friction velocity, and is defined as

$$v_\tau = \left(\frac{\tau_w}{\rho}\right)^{\frac{1}{2}}. \tag{25}$$

b) There should be at least 10 cells within the viscosity-affected near-wall region $(Re_x < 200)$ to be able to resolve the mean velocity and turbulent quantities in that region.

A comprehensive study was undertaken to determine the grid sizes, time steps and iteration convergence criteria. As an outcome of the grid independence study, a non-uniform grid size was chosen as follow: 120 × 100 (for $H/d = 5$), 120 × 140 (for $H/d = 7$) and 120 × 180 (for $H/d = 9$) in the axisymmetric domain, thus satisfying the near-wall meshing condition as discussed above. A finer grid is taken near the wall and the air jet region of the domain, while a coarser grid system is used far away from the boundary layer.

It is found that time step has a profound effect on the convergence of the solution in this periodic problem. An appropriate time step which ensured a converged solution without costing excessive computational time was determined following a series of studies, and the following time step was chosen accordingly:

$$\Delta t = \frac{T}{20} \tag{26}$$

where T is the time period of the waveform of the jet.

Convergence in inner iterations is declared only when the scaled residual (R^Φ) is decreased to 10^{-4} for all equations except the energy equation, for which the criterion is 10^{-6}. So (R^Φ) is defined for all governing equations (except the continuity equation) as

$$R^\Phi = \frac{\sum_{cellsP} \left| \sum_{nb} a_{nb}\Phi_{nb} + b - a_p\Phi_p \right|}{\sum_{cellsP} |a_p\Phi_p|} \tag{27}$$

where Φ_p stands for each variable u, v, T, k and ε at grid point P, a_p a is coefficient and a_{nb} are the neighbouring coefficients in the discretization equation.

The scaled residual for the continuity equation is defined as

$$R^\Phi = \frac{R^c_{\text{iterationN}}}{R^c_{\text{iteration5}}} \quad \text{and}$$
$$R^c = \sum_{\text{cellsP}} |\text{rate of mass creation in cell } P|. \tag{28}$$

The denominator is the largest absolute value of the continuity residual in the first five iterations.

IV. Results and Discussion

The present model is validated using the results of Mladin and Zumbrunnen [5], who performed experiments with pulsating planar jets with nozzle dimensions 5 × 50 mm. This was approximated as a 2-D planar jet for the purpose of model validation in the present work, as the high-aspect-ratio nozzle used in [5] is expected to behave like a 2-D jet. Similar validation exercise was also performed using numerical and experimental results presented in Ichimiya and Hosaka [16], [17] for steady jets. The results of validation are shown in Figs. 4 and 5, respectively. The Nusselt number variation is taken as a measure of compliance. The qualitative behavior is well replicated in both the cases. The quantitative differences can be attributed to 3-D effects in slot jets which are approximated by an equivalent 2-D planar jet. Since a reasonable compliance is obtained, the model is used to characterize the pulsating jets as means of enhancing heat transfer. Subsequent simulations for round jets were carried out with an axisymmetric nozzle for the present study. Inter alia, a parametric study is carried out to quantify the effect of each of them. The parameters considered are the Reynolds number of the jet, nozzle-to-wall spacing, and frequency, amplitude and wave form of the pulsations. All results presented here pertain to steady periodic conditions.The properties of air used in this study are enumerated in Table I.

Flow characterization of pulsated impinging jets: Fig. 6 shows the variation of maximum radial velocity with time for different waveforms of the pulsated impinging jets over

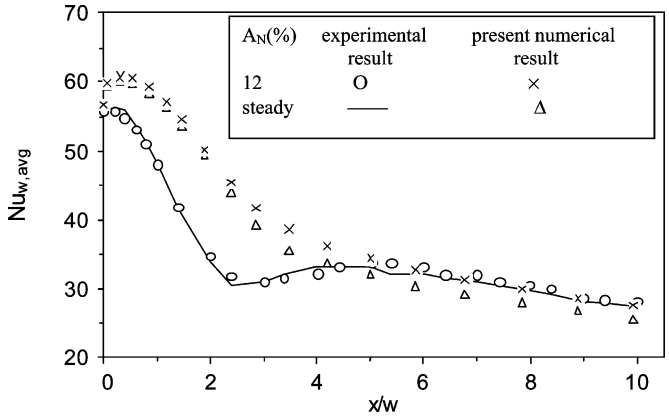

Fig. 5. Comparison of time-averaged Nusselt number with experimental results [5] for $Re_w = 11000$, $f = 23$ Hz, $H/w = 5$ and $q = 5000$ Wm^{-2}.

TABLE I
PHYSICAL PROPERTIES OF AIR AND SYSTEM DATA

Properties	
Density (ρ)	1.225 kg m^{-3}
Dynamic viscosity (μ)	1.7894×10^{-5} N s m^{-2}
Thermal conductivity (K)	0.0242 W m^{-1} K^{-1}
Specific heat (c_p)	1006.43 J kg^{-1} K^{-1}
Atmospheric temperature (T_∞)	300 K
System data	
Diameter of nozzle (d)	0.005 m
Length of the wall (L)	0.025 m
Heat flux (q)	6000 W m^{-2}

a single time period. Fig. 6(a) corresponds to a sinusoidal jet and Fig. 6(b) to a square wave jet. The common features of pulsated jets and steady jets are the increase in the maximum radial velocity up to $r/d = 1$, then followed by a decrease. The distinguishing features are that the temporal variations in radial velocity broadly follow the wave form of the input jet but with a smearing effect towards the end of the time period.

Fig. 7 shows a comparison of the of time-averaged maximum radial velocity variation along the wall for different waveforms of pulsated impinging jets. It can be observed that the time-averaged maximum radial velocity variation is higher in pulsated jets, in general, and augmentation is more for a square wave than for a sine wave jet.

Fig. 8 shows the variation of hydrodynamic boundary layer thickness (Δ) with time for different r/d values for a square wave jet for two time periods. The hydrodynamic boundary layer thickness is defined as the distance from the wall where the radial velocity becomes half the local maximum velocity, i.e., where velocity becomes $v_{\max}/2$ (see Fig. 1). The boundary layer thickness decreases initially for r/d value from 0 to 2, and then it increases with a further increase in r/d. In addition, the sharp peaks continually become blunt with increase in r/d.

Fig. 9 shows the variation of time-averaged hydraulic boundary layer thickness (Δ_{avg}) along the wall for different frequencies of the square wave jet. It is found that the boundary

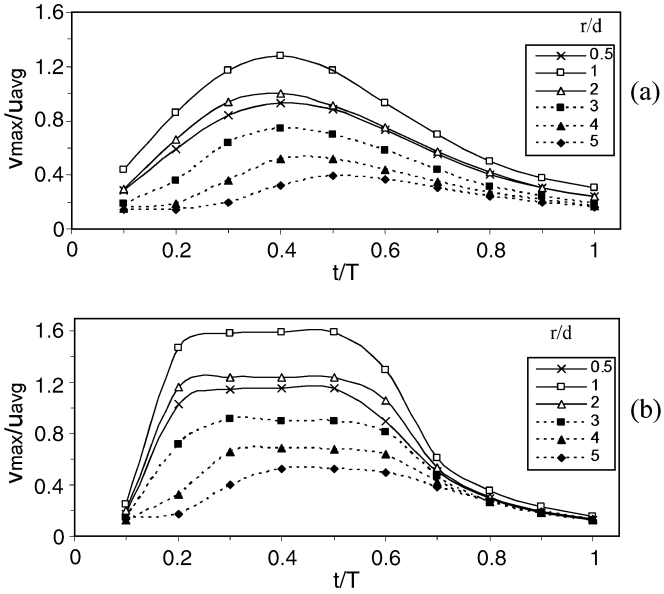

Fig. 6. Variation of maximum radial velocity with time for $Re = 5130$, $f = 50$ Hz, $A_N = 47\%$ and $H/d = 5$: (a) sine wave jet and (b) square wave jet.

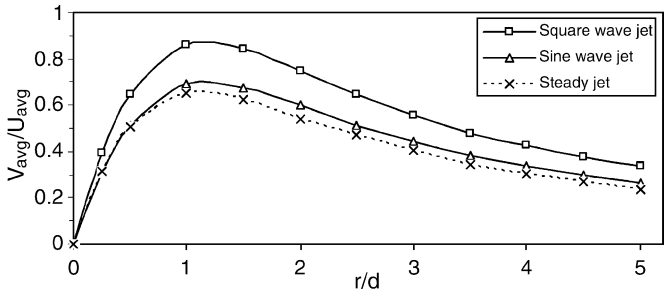

Fig. 7. Comparison of time-averaged radial velocity variation along the wall for $Re = 5130$, $A_N = 47\%$, $f = 100$ Hz, and $H/d = 7$.

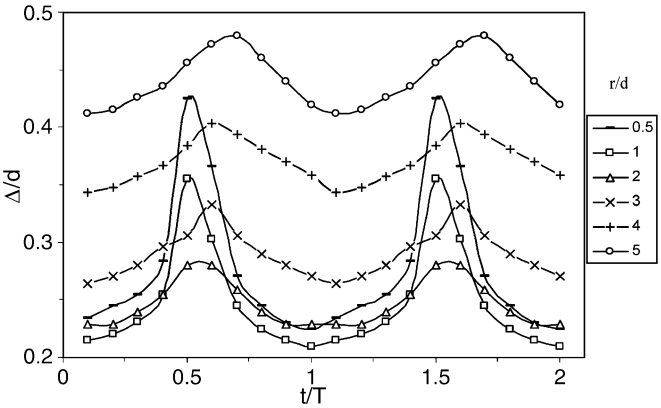

Fig. 8. Variation of hydrodynamic boundary layer thickness with time for square wave jet of $Re = 5130$, $f = 400$ Hz and $H/d = 7$.

layer thickness along the wall decreases with increase in frequencies ($100 < f < 400$). Hence it can be inferred that a high frequency square wave jet will result in a reduced resistance to heat transfer at the wall.

Results for the steady jets: In order to establish a base line against which on can compare the results of pulsating jets, in the first instance, Nusselt number variations along the wall with

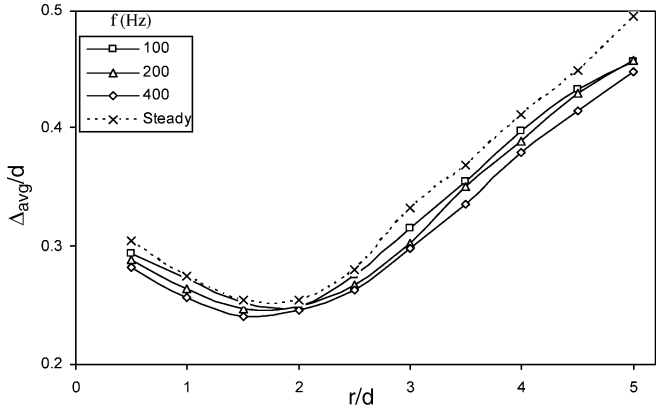

Fig. 9. Variation of time-averaged hydrodynamic boundary layer thickness along the wall for square wave jets of $Re = 5130$ and $H/d = 7$.

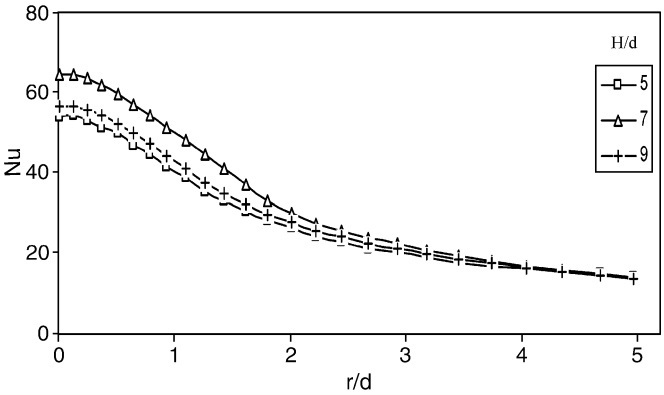

Fig. 10. Variation of Nusselt number along the wall for steady jets of $Re = 5130$.

steady jets are computed. One of the most important characteristics of the submerged jets is the existence of a shear layer between the pre-impingement jet and the ambient fluid. Heat transfer is sensitive to the nozzle-to-wall spacing, especially if the impingement surface is held beyond the end of potential core (i.e., $H/d > 4$). Immediately after leaving the nozzle, the jet begins to entrain the surrounding stagnant fluid. However, prior to reaching the end of the potential core, the center line velocity of the jet is unaffected by mixing and remains the same as the nozzle exit velocity. Fig. 10 shows the variation of Nusselt number along the wall for steady jets of different H/d values. The Nusselt number is found to increase with an increase in H/d and it reaches peak value at about $H/d = 7$. The increase in the Nusselt number can be attributed to an increase in the free stream turbulence intensity due to interaction between the jet and the stagnant surrounding. The Nusselt number decreases with increasing H/d beyond 7. This suggests acceleration in the degeneration of flow structures [5].

Results for the square wave jets: Fig. 11 shows the variation of time-averaged Nusselt number with r/d for different frequencies of the intermittent jets for an H/d ratio of 7. The variation of Nusselt number for the steady jet is shown for the sake of comparison. In Fig. 11(a) for $Re = 5130$, the Nusselt number for a low frequency pulsating jet ($f = 50$ Hz) is found to be lower in the stagnation region than for a steady jet. This diminution occurs because the enhancement of cooling due boundary layer renewal is not enough to offset the effects of reduction in cooling due to the absence of coolant during the off cycle. However, as the frequency is increased, enhancement in the Nusselt number becomes apparent along the entire length of the wall. In Fig. 11(b) with a higher Reynolds number ($Re = 6850$), the impact of pulsations on Nusselt number is realized only at a higher frequency ($f > 100$ Hz). Fig. 11(c) for $Re = 8560$, reaffirms this feature. The rate of enhancement in the Nusselt number is found to decrease in the stagnation region for higher frequencies of the intermittent jets as compared to that of steady jet. It suggests that the response of new boundary layer formation may be slow in the stagnation region for the intermittent jets of high Reynolds number, because the boundary layer is already quite thin there.

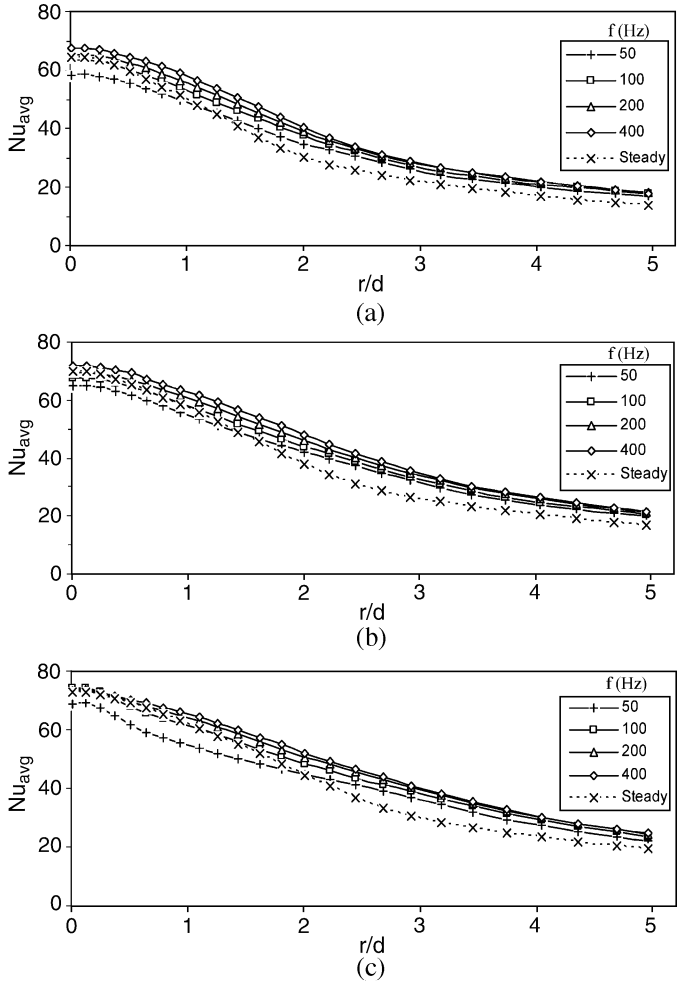

Fig. 11. Variation of time-averaged Nusselt number along the wall for square wave jets with $H/d = 7$: (a) $Re = 5130$, (b) $Re = 6850$ and (c) $Re = 8560$.

Fig. 12 shows the variation of time-averaged stagnation point Nusselt number with Reynolds number for different frequencies ($50 < f < 400$ Hz) of intermittent jets. A common feature is that there is an increase in the time averaged Nusselt number in the stagnation region for Reynolds numbers up to 7000 at frequencies greater than about 200 Hz. Fig. 12(b) is for $H/d = 7$, which is about optimum height for a steady jet. It appears that, high Reynolds numbers and high frequencies of interruptions need not result in proportional enhancement of Nusselt number.

The degradation of the coherent structure of the intermittent jet is due to two features, namely the natural turbulence (governed by the Reynolds numbers) and the temporally promoted

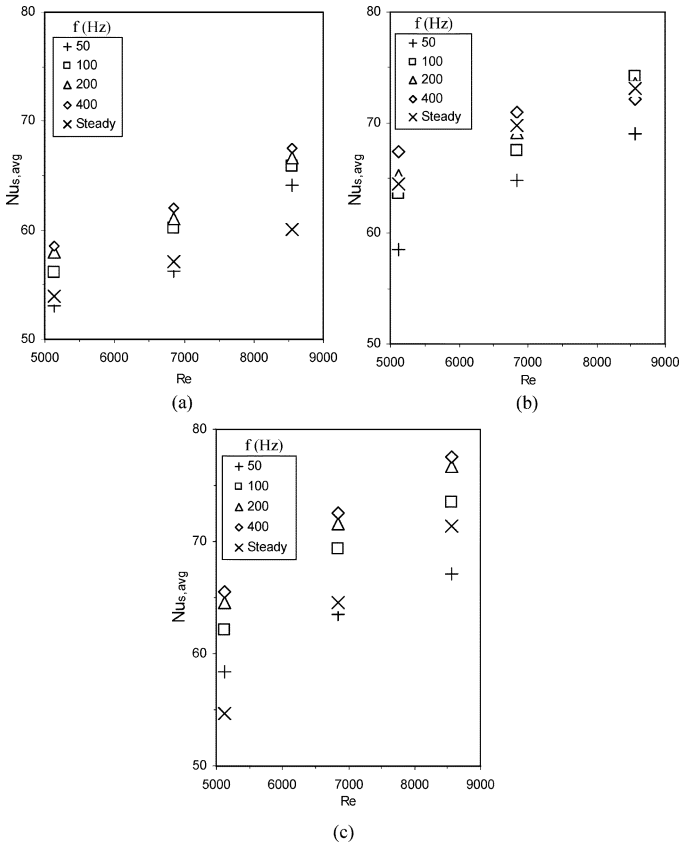

Fig. 12. Variation of time-averaged stagnation point Nusselt number with Reynolds number for square wave jets: (a) $H/d = 5$, (b) $H/d = 7$, and (c) $H/d = 9$.

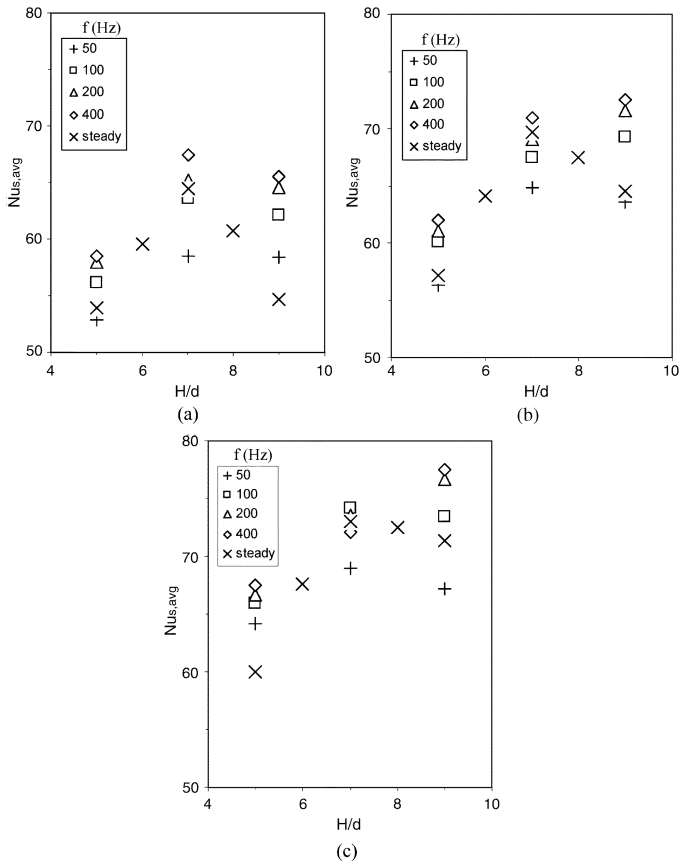

Fig. 13. Variation of time-averaged stagnation point Nusselt number with nozzle-to-wall spacing (H/d) for square wave jets: (a) $Re = 5130$, (b) $Re = 6850$, and (c) $Re = 8560$.

turbulence [9]. If there is adequate turbulence provided by the natural turbulence, the cumulative effect due to temporal imposition is marginal. On the other hand at lower natural turbulence levels, time domain disturbances promote the degradation. This could possibly explain the qualitative enhancement of heat transfer as a function of Reynolds number and the frequency of interruptions. Thus, for the case of low-Reynolds-number turbulent flow, it is found that the pulsation of jet has a significant effect on the Nusselt number enhancement. However, for the case of high-Reynolds-number turbulent flow which is characterized by high turbulent kinetic energy, the enhancement of Nusselt number due to jet interruption is not very significant.

Fig. 13 shows the variation of time-averaged stagnation point Nusselt number with wall-to-nozzle spacing (H/d) for different frequencies $(25 < f <400$ Hz) of the intermittent jets. One common feature is that the steady jet has an optimal H/d of about 7. This is also depicted by periodic jets at low frequencies ($f <100$ Hz). But, at frequencies higher than this value, it is possible to enhance the Nusselt number by increasing the Reynolds number, although the magnitude of enhancement may not be commensurate with the same in Reynolds number and frequency. This leads to the inference that, in a practical application, use of frequencies in excess of 250 Hz and Reynolds number greater than about 6000 and $H/d >7$ are unlikely to provide additional benefits.

Results for the sine wave jets: Fig. 14 shows the variation of time-averaged Nusselt number with r/d for different amplitude and frequency of sine wave jets. At low values of A_N [23%-Fig. 14(a)], there is virtually no benefit over a steady jet. As the value of A_N increases, [Fig. 14(b) and (c)], the benefit of pulsing gradually emerges. This result suggests that, at low A_N, the pulses are not strong enough to trigger natural instabilities which is also suggested by Mladin and Zumbrunnen [6]. At values higher than about $A_N = 40\%$, the increase in the free stream turbulence intensity seem to augment the Nusselt number. Thus, as the amplitude of pulses increases, destabilization of the hydrodynamic boundary layer also increases in the wall jet region. The Nusselt number decreases in the stagnation region as compared to that of steady jet. This result suggests that, due to the nonlinear dynamic effects, the time-averaged thermal and hydrodynamic layer thicknesses are greater than the corresponding values of the steady jet [3], [11].

Fig. 15 shows the variation of time-averaged stagnation point Nusselt number with nozzle-to-wall spacing for different frequencies $(50 < f <250$ Hz)of the pulsating jets. For $H/d = 5$ and 9, and all amplitude ranges ($A_N = 23\%$, 35%, 47%), the Nusselt number increases with increase in frequency ($f >100$ Hz) as compared to the steady jet. But, at about $H/d = 7$, which is approximately the optimal range for a steady jet, the effect of frequency and A_N is non-intuitive. The augmentation seems to take effect only for $A_N >40\%$.

Comparison of square and sine wave jets: Fig. 16 shows an assessment of the percentage for increase in time-averaged Nusselt number (w.r.t. the steady value) along the wall for different waveforms of jet. For square wave jet with $Re = 6850$,

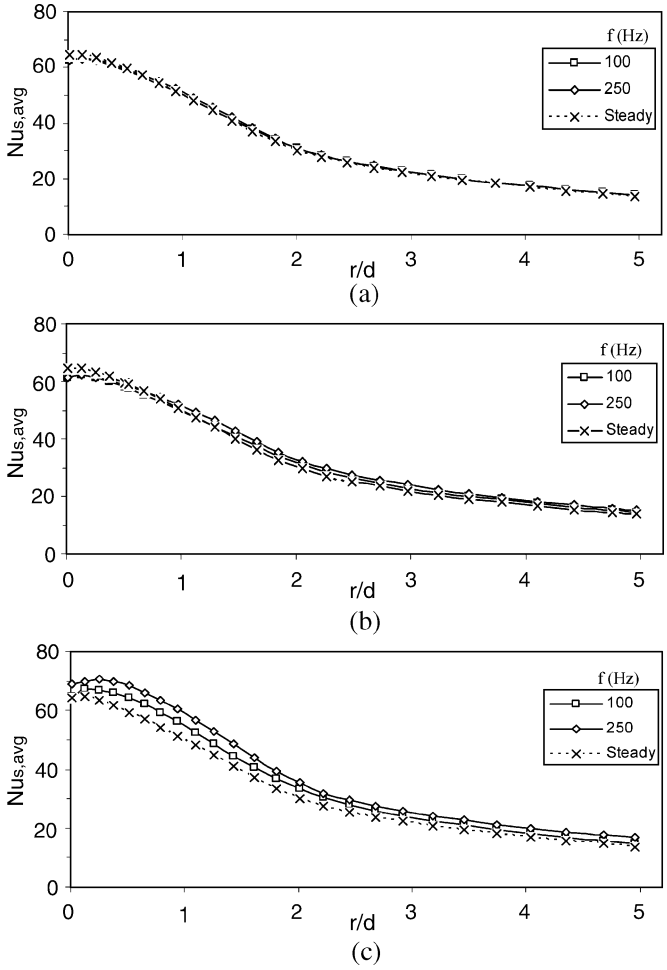

Fig. 14. Variation of time-averaged Nusselt number along the wall for sine wave jets with $Re = 5130$ and $H/d = 7$: (a) $A_N = 23\%$, (b) $A_N = 35\%$, and (c) $A_N = 47\%$.

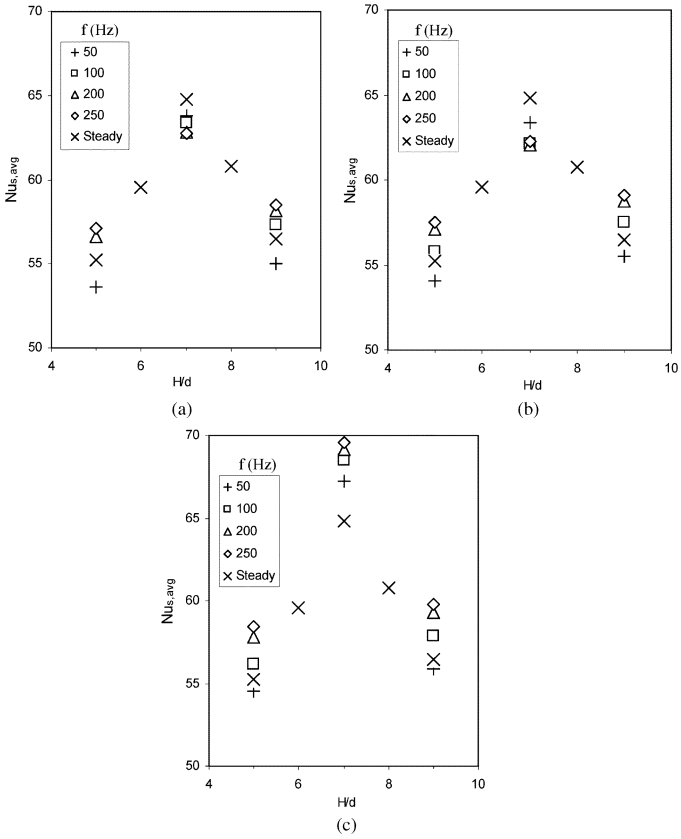

Fig. 15. Variation of time-averaged stagnation point Nusselt number with nozzle-to-wall spacing (H/d) for sine wave jets with $Re = 5130$: (a) $A_N = 23\%$, (b) $A_N = 35\%$, and (c) $A_N = 47\%$.

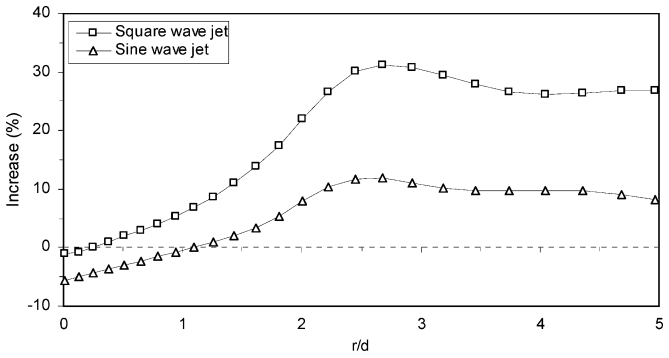

Fig. 16. Variation of percentage for increase in time-averaged Nusselt number along the walll for $Re = 6850$, $f = 200$ Hz, $A_N = 53\%$ and $H/d = 7$.

$f = 200$ Hz, and $H/d = 7$, the enhancement is appreciably higher than for a sine wave jet. The maximum benefit is seen at an r/d value of about 2.5 (up to 30% for square and 10% for sine wave jet). Then, there is a marginal decrease followed by a plateau. This reaffirms the earlier observation that the augmentation arises due to a reduced average thickness of boundary layer as depicted in Fig. 9. The initial steep rise can be attributed to instabilities caused by pulsing and reduction in average thickness of boundary layer. But, for $r/d >$ about 3, the boundary layer fluctuations are not that significant (Fig. 8). Yet, the augmentation level seems to remain the same. Possibly, this could be due to turbulence increase caused by temporal disturbances.

V. Conclusion

This paper is focused on the possible improvements to heat transfer with pulsated impinging jets. A numerical model is developed for simulating heat transfer and fluid flow with $k - \varepsilon$ turbulence model. For the case of steady jet, with all Reynolds numbers, the Nusselt number is found to reach a peak value at about $H/d = 7$. For the case of a square wave jet with $Re = 5130$ and $H/d = 7$, the time-averaged Nusselt number increases by up to 12% in the stagnation zone and 35% in the wall jet zone in the frequency range ($25 < f < 400$ Hz) as compared to that of the steady jet. It is found that, Reynolds numbers above 7000 and frequencies above 250 Hz need not necessarily result in appreciable enhancement of Nusselt number. For the case of a sine wave jet with the same $Re = 5130$ and $H/d = 7$, the time averaged Nusselt number increases by up to 5% in the stagnation zone and 10% in the wall jet zone in the frequency ($50 < f < 250$ Hz) and amplitude ($23 < A_N < 47\%$) as compared to that of the steady jet. It is concluded that, the dominant feature for augmenting heat transfer is the amplitude and not the frequency.

The results of the parametric investigation reported here clearly exhibit that the pulsated impinging jet enhances the performance impinging jets. Hence, these designs can be utilized to enhance heat transfer for cooling of electronic systems.

REFERENCES

[1] B. W. Webb and C. F. Ma, "Single-phase liquid jet impingement heat Transferv," in *Advances in Heat Transfer*, J. P. Hartnett, T. F. Irvine, Y. I. Cho, and G. A. Greene, Eds. New York: Academic, 1995, vol. 26, pp. 105–208.

[2] R. J. Goldstein, E. R. G. Eckert, W. E. Ibele, S. V. Patanker, T. W. Simon, T. H. Kuehn, P. J. Strykowski, K. K. Tamma, J. V. R. Herberlein, J. H. Davidson, J. Bischof, F. A. Kulacki, U. Kortshagen, and S. Garrick, "Heat Transfer—A review of 2001 literature," *Int. J. Heat Mass Transf.*, vol. 46, pp. 1887–1992, 2003.

[3] E. C. Mladin and D. A. Zumbrunnen, "Nonlinear dynamics of laminar boundary layers in pulsate stagnation flows," *J. Thermophys. Heat Transf.*, vol. 8, pp. 514–523, 1994.

[4] D. A. Zumbrunnen and M. Aziz, "Convective heat transfer enhancement due to intermittency in an impinging jet," *Trans. ASME, J. Heat Transf.*, vol. 115, pp. 91–98, 1993.

[5] E. C. Mladin and D. A. Zumbrunnen, "Local convective heat transfer to submerged pulsating jets," *Int. J. Heat Mass Transf.*, vol. 40, pp. 305–3321, 1997.

[6] E. C. Mladin and D. A. Zumbrunnen, "Alterations to coherent flow structures and heat transfer due to pulsations in an impinging air jet," *Int. J. Therm. Sci.*, vol. 39, pp. 236–248, 2000.

[7] H. S. Sheriff and D. A. Zumbrunnen, "Means to improve the heat transfer performance of air jet arrays where supply pressure is limiting," *Trans. ASME, J. Heat Transf.*, vol. 120, pp. 787–789, 1998.

[8] H. S. Sheriff and D. A. Zumbrunnen, "Local and instantaneous heat transfer characteristics of arrays of pulsating jets," *Trans. ASME, J. Heat Transf.*, vol. 121, pp. 341–348, 1999.

[9] H. S. Sheriff and D. A. Zumbrunnen, "Effect of flow pulsations on the cooling effectiveness of an impinging jet," *Trans. ASME, J. Heat Transf.*, vol. 116, pp. 886–895, 1994.

[10] D. J. Sailor, D. J. Rohli, and F. Qianli, "Effect of variable duty cycle flow pulsations on heat transfer enhancement for an impinging air jet," *Int. J. Heat Fluid Flow*, vol. 20, pp. 574–580, 1999.

[11] H. S. Sheriff and D. A. Zumbrunnen, "Dependence of heat transfer to a pulsating stagnation flows on pulsation characteristics," *J. Thermophys. Heat Transf.*, vol. 9, pp. 181–192, 1995.

[12] *"FLUENT 6.0, User's and Tutorial Guide,"* Fluent, Inc., 2002.

[13] M. Wolfstein, "The cvelocity and temperature distribution of one-dimensional flow with turbulence augmentation and pressure gradient," *Int. J. Heat Mass Transf.*, vol. 12, pp. 301–318, 1969.

[14] H. C. Chen and V. C. Patel, "Near-wall turbulence models for complex flows including separation," *AIAA J.*, vol. 26, pp. 641–648, 1988.

[15] H. K. Versteeg and W. Malalasekera, *An Introduction to Computational Fluid Dynamics—The Finite Volume Method*. London, U.K.: Longman Scientific and Technical, 1995.

[16] K. Ichimiya and N. Hosaka, "A fundamental study of heat transfer characteristics due to confined impinging two-dimensional jets Numerical estimation for three laminar slot jets," *Trans. JSME B*, vol. 56, pp. 1727–1732, 1990.

[17] K. Ichimiya and N. Hosaka, "Experimental study of heat transfer characteristics due to confined impinging two-dimensional jets," *Exper. Therm. Fluid Sci.*, vol. 5, pp. 803–807, 1992.

Ramesh Chandra Behera received the B.S. degree from the College of Engineering and Technology, Bhubaneswar, India, in 1996 and the M.S. degree from the Indian Institute of Science, Bangalore, in 2003.

His main research area is computational fluid dynamics and heat transfer.

Pradip Dutta received the Ph.D. degree from Columbia University, New York, NY, in 1992.

He is an Associate Professor in the Department of Mechanical Engineering, Indian Institute of Science, Bangalore. His main research areas include computational heat transfer and fluid flow, transport phenomena in materials processing, and thermal management of electronic systems.

Dr. Dutta is a Fellow of the Indian National Academy of Engineering.

K. Srinivasan received the M.S. degree from the Indian Institute of Technology, Madras, in 1974 and the Ph.D. degree from The Australian National University, Canberra, in 1981.

He is a Professor in the Department of Mechanical Engineering, Indian Institute of Science, Bangalore. His main research areas include adsorption refrigeration and development of cooling technologies for electronic systems.

Dr. Srinivasan is a Fellow of the American Society of Mechanical Engineers (ASME).